



Micro-mechanism and efficiency of baffle structure in deceleration of granular flows

Bei Zhang¹ · Yu Huang^{1,2} · Jie Liu¹

Received: 15 October 2020 / Accepted: 26 June 2021 / Published online: 10 July 2021
© The Author(s), under exclusive licence to Springer-Verlag GmbH Germany, part of Springer Nature 2021

Abstract

Baffle system is a promising disaster mitigation measure, while the mechanism of debris-baffle interaction at grain scale has not been fully understood, and especially the effect of the unsteady nature of granular flow on debris-baffle interaction has not been detailly investigated. For this purpose, we conducted various small-scale model tests and used the three-dimensional discrete element method to assist the interpretation of the experimental results and extend research content. The granular arch that is formed between the baffle slit controls the debris-baffle interaction, which is completely different from the dead zone-dominant debris-barrier interaction mechanism represented by a rigid or flexible barrier. The particle size effect is controlled by the baffle jamming behavior. Larger particles facilitate the rapid formation of a stable force arch with larger energy-breaking efficiency. And flows with larger Froude number are not easy to form stable granular arches. Thus, the baffle array number, particle size, and construction site control the efficiency of baffle structure in deceleration of granular flows. Particularly, increasing the baffle array number restricts the recovery of flow mobility after the flow passes the baffle structure. In general, the construction of baffle at deposition area may not be an effective engineering options, because the impact force discrepancy on baffle array is larger by 28%, the generated energy dissipation is lower by 60.97%, the run-out distance by 10% and the spreading distance on the slope by approximately 40% for baffles in the deposition area compared with baffles constructed on slope.

Keywords Debris-baffle interaction · Discrete element method · Deposition · Energy dissipation · Granular flow · Run-out

1 Introduction

Natural granular flow is a catastrophic geological disaster [13]. In some cases, such as the 2010 Zhouqu debris flow [16] and 2015 Guangming landslide [40], granular flows have caused a large number of human casualties and

tremendous economic losses. Disaster mitigation studies have attracted a great amount of attention among the scientific community [4, 17, 30]. Engineering structures, such as check dams, are widely used in the field to reduce the destructivity of granular flows [29]. These structural countermeasures are crucial for the safety of human settlements and other important infrastructures, particularly in mountainous areas. However, these closed structure types can easily be destroyed owing to the powerful effect exerted by granular flows on the structures [15]. Additionally, their maintenance is very costly because the barrier loses its function after being buried by deposition. Hence, the adoption of open structures is preferable in the field recent years. Flexible barriers, because of lower stiffness and partial retention of granular material [2, 28, 38], have been proved as a promising disaster protection measures as the impact load especially generated by boulders could be largely attenuated [33]. Open

✉ Yu Huang
yhuang@tongji.edu.cn

Bei Zhang
beizhang@tongji.edu.cn

Jie Liu
oucliujie@tongji.edu.cn

¹ Department of Geotechnical Engineering, College of Civil Engineering, Tongji University, Shanghai 200092, China

² Key Laboratory of Geotechnical and Underground Engineering of the Ministry of Education, Tongji University, Shanghai 200092, China

silts allow a portion of material to escape the barrier; thus, the load on the barrier and the deposition behind the barrier are reduced. By careful design, open barrier types can achieve better performance compared with closed barrier types [14, 24, 41].

In recent years, the baffle array, which is an open barrier type, has attracted a great amount of interest among the scientific and engineering communities because it is a promising structure for decelerating granular flows and thereby reducing their destructive power. Ng et al. [27] conducted a series of physical tests to investigate the reduction of the flow velocity of a granular flow after the passing the baffle structure and concluded that the three baffle arrays reduced the frontal velocity by 57%. Based on a large number of physical tests and numerical simulations, the optimal baffle space, height, and array distance have been identified [10, 21]. Bi et al. [6] investigated the effect of the baffle structure on the run-out and impact behavior of a rock avalanche under a hypothetical prototypical condition. Wang et al. [39] demonstrated that arc-shaped baffles are effective in regulating the rock avalanche deposition. Li et al. [23] developed a new numerical tool based on the material point method to assist in the rational design of baffle structures. The abovementioned studies have mainly focused on optimizing the baffle configuration by changing the baffle height, shape, column spacing, or array distance. Additionally, the reduction of the flow velocity, run-out distance, or deposition area has been set as indicators.

Although previous studies have reported many remarkable results, a general design criterion for baffle structures has not been fully established to date, because various issues have not been satisfactorily solved. One of the biggest is that the mechanism of debris-baffle interaction at grain scale has not been fully understood. The main research gap lies in the unsteady nature of granular flow has not been detailly investigated when addressing debris-baffle interaction. On the other hand, a fully developed granular flow disaster mainly comprises three stages: the slope failure process, granular debris surging downslope (acceleration) and deposition (deceleration), and at different stage, the Froude characteristic of granular flow could be different, which is crucial for barrier design. For example, Ng et al. [26] revealed that the flow-thinning process of granular flow when surging downslope exerts a profound effect on impact and run-up on barrier. And Chen et al. [8] adopted a simulation-based approach to optimize the barrier position against debris flow disaster. Various studies have investigated baffles constructed on a slope, where the granular flow is accelerated [6, 10, 27], while others have investigated baffles constructed in the deposition area where the granular flow undergoes deceleration [39]. However, the effect of Froude characteristic on

debris-baffle interaction has not been properly addressed. On the other hand, the unsteady nature of granular flow also comes from its material composition, and further when passing a narrow spacing, particle size could exert an important effect [3, 5, 18]. And thus, the jamming effect of baffle structure should be investigated considering particle size, which is properly covered previously.

To assist the development of reliable baffle systems, we designed various small-scale model tests, and used the three-dimensional (3D) discrete element method (DEM) to back-analyze and assist the interpretation of the experimental results. The two above-mentioned issues were thoroughly investigated by considering the particle size of the granular debris and the effect of the construction site. Notably, the construction site effect was simplified by considering that the baffle is installed at the granular acceleration path or deceleration path. The findings of this study could strengthen the understanding of debris-baffle interaction and improve the reliability of baffle design in the field.

2 Methodology

2.1 Physical tests

Fume modelling of granular flow impact has been demonstrated as effective tool in understating of flow-structure interaction mechanism [20, 25, 37]. Thus, a small-scale flume model was designed including a material storage container, inclined flume with a front opening, and deposition area. As shown in Fig. 1a, the material storage container had a length of 15 cm, height of 12 cm, and width of 10 cm. The total length of the flume was 80 cm, and the spreading length of the material was 65 cm. The width and height of the flume were 10 cm and 12 cm, respectively. A flat plane was installed at the end of the flume and was sufficiently large to allow the full deposition of granular flow. The flume was made using high density polyethylene (HDPE) and was inclined at 45° to form a rapid granular flow. This slope angle was fixed in all cases.

The baffle was also constructed using the HDPE material because structural failure was not considered in this study. As shown in Fig. 1a and b, the baffle arrays were installed at two positions: position 1 refers to the acceleration stage of the granular flow, and position 2 refers to the deceleration stage (deposition stage). At position 1, the effect of the number of baffle arrays (R_1 , R_2 , R_3) was considered. The baffle configuration is presented in Fig. 1a. This part of the study was carried out using physical modelling. At position 2 (Fig. 1b), a similar test program was adopted and carried out using numerical modelling. The baffle used in our experiment had a square shape with

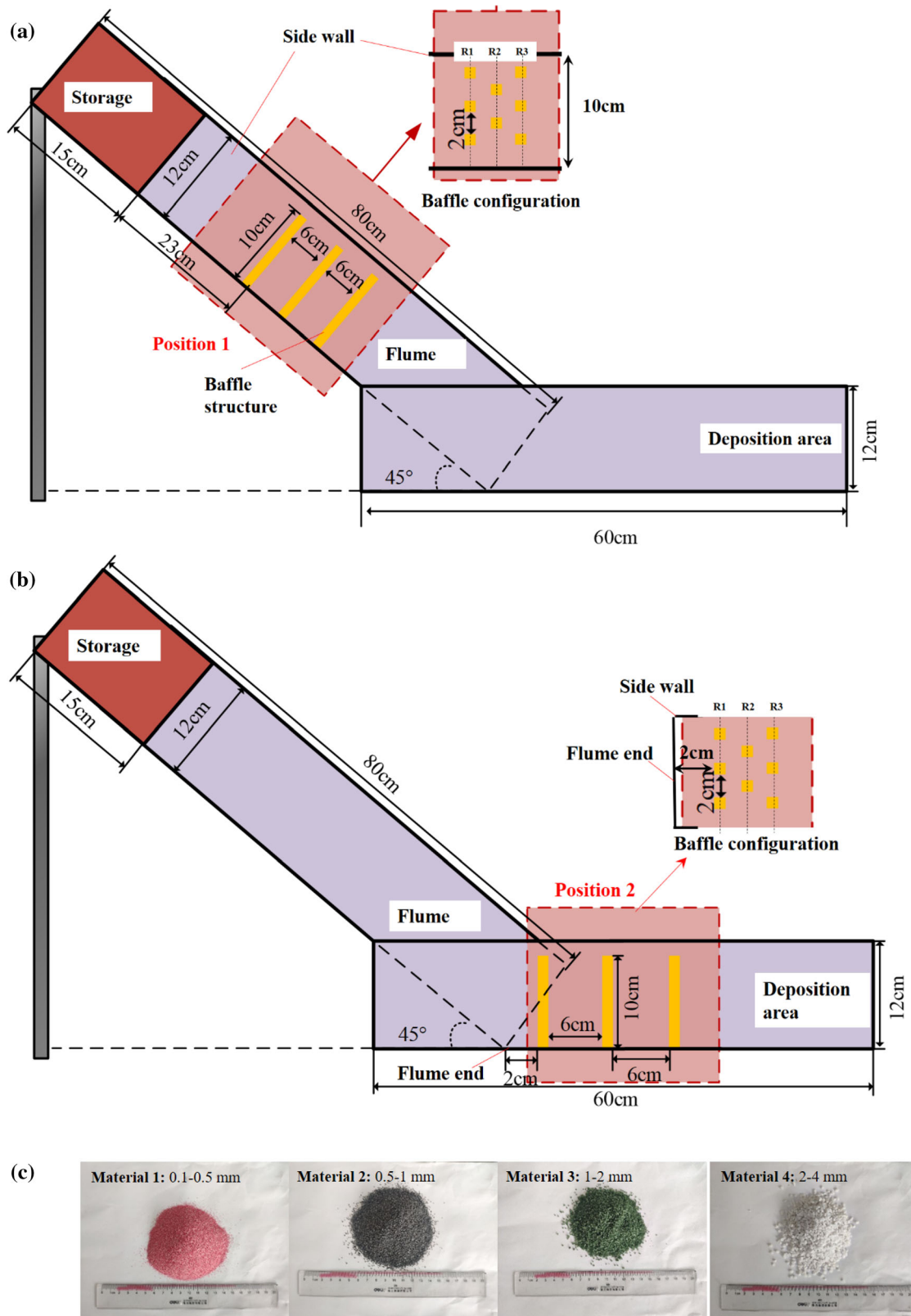


Fig. 1 Flume configuration and test materials

a dimension of 1 cm and height of 10 cm. The baffle spacing was 2 cm and the array spacing was 6 cm. In this study, the baffle or array spacing did not vary and only the baffle array number was considered.

In the physical modelling carried out in this study, four types of granular material with different particle size were considered: 0.1–0.5 mm (material 1), 0.5–1 mm (material 2), 1–2 mm (material 3), and 2–4 mm (material 4), as shown in Fig. 1c. The internal friction angle of the granular material was measured by a cylinder lifting test and dam break test, according to the literatures [6, 31]. Additionally, the interface friction angle was measured by tilting tests as described by Jiang and Towhata [20]. The results and other physical properties of the used granular material are presented in Table 1. Initially, the granular material was filled into the storage container using the pluvial deposition method [20] to form a rectangular deposition shape with the dimension of 15 × 10 × 8 cm. The material mass was controlled to generate similar initial deposition bulk density, which has been observed to exert a noticeable influence on the flow impact dynamics [1]. The material was released by a mechanical gate to initiate a dam break failure and then formed a granular flow. A high-speed camera with a frame rate of 240 frames per second was used to capture the flow kinematics during the debris-baffle interaction. Thus, the velocity reduction caused by the deceleration induced by the baffle structure was obtained using PIV analysis [35].

To investigate the micro-mechanism and efficiency of the baffle structure with regard to the deceleration of granular flows, a total of 23 tests were conducted, including 16 physical modeling tests and 7 DEM simulation tests, as presented in Table 2. Overall, the particle size effect, baffle number, and baffle installation position were considered to achieve the objective of this study.

2.2 Numerical simulations

The DEM simulation was conducted to elucidate the micro-mechanism of the debris-baffle interaction and

further analyze the effect of the baffle’s installation position. The DEM has already been demonstrated as an effective tool for dealing with granular flows and offering various fundamental insights particularly with regard to flow-structure interaction [3, 6, 10, 12, 14, 21, 22, 41]. In DEM simulation, the granular material was represented by discrete spherical particles, and the baffle and flume were built using wall elements.

The commercial software EDEM was used to conduct the simulation. The numerical model was built according to the physical model shown in Fig. 1. The simulation was divided into three stages: the material preparation, debris-baffle interaction, and run-out. In the first stage, the particles were generated in the particle factory and deposited while being freely driven by gravity (9.81 m/s²). Subsequently, a plate was used to press the generated particles with a slow velocity and form a continuous granular body with the dimension of 15 × 10 × 8 cm, which is identical to the granular body considered in the physical tests. A trigger gate was used to simulate the dam break failure model until all particles reaching static, and the granular flow was thus formed. Under the traction of gravity (9.81 m/s²), the particles surged downslope and interacted with the baffles. Next, the particles were gradually deposited onto the sliding surface and deposition area.

In the DEM simulation, it was important to calculate the micro-contact force between the particles or between the particles and the geometry (flume or baffle). The EDEM offers an effective model called Hertz-Mindlin (no slip) for calculating the normal contact force (F_n) and tangential contact force (F_t) as follows:

$$F_n = F_n^c + F_n^d = \frac{4}{3} \cdot E^* \sqrt{R^*} \delta_n^{\frac{3}{2}} - 2 \cdot \sqrt{\frac{5}{6}} \cdot \gamma \cdot \sqrt{S_n m^*} v_n^{rel} \tag{1}$$

$$F_t = \min \{ F_t^c + F_t^d, \mu F_n \} \\ = \min \left\{ S_t \delta_t + 2 \cdot \sqrt{\frac{5}{6}} \cdot \gamma \cdot \sqrt{S_t m^*} v_t^{rel}, \mu F_n \right\} \tag{2}$$

E^* , G^* , R^* , and m^* are the equivalent Young’s modulus,

Table 1 Physical properties of granular materials used in experimental tests

Material ID	Particle diameter d_p (mm)	Minimum dry unit density $\rho_{d\min}$ (g/cm ³)	Maximum dry unit density $\rho_{d\max}$ (g/cm ³)	Internal friction angle μ_0 (°)	Interface friction angle μ_1 (°)
PSD1	0.1–0.5	1.28	1.63	31	28
PSD2	0.5–1	1.34	1.62	30	27
PSD3	1–2	1.37	1.60	31	27
PSD4	2–4	1.37	1.56	31	30

Table 2 Program of physical tests and numerical simulations

Test ID	Test material	Baffle row number	Baffle installation position	Test technology
1	PSD1	–	–	Physical modeling
2	PSD2	–	–	Physical modeling
3	PSD3	–	–	Physical modeling
4	PSD4	–	–	Physical modeling
5	PSD4	–	–	Numerical simulation
6	PSD1	1 (R1)	Position 1	Physical modeling
7	PSD1	2 (R1 + R2)	Position 1	Physical modeling
8	PSD1	3 (R1 + R2 + R3)	Position 1	Physical modeling
9	PSD2	1 (R1)	Position 1	Physical modeling
10	PSD2	2 (R1 + R2)	Position 1	Physical modeling
11	PSD2	3 (R1 + R2 + R3)	Position 1	Physical modeling
12	PSD3	1 (R1)	Position 1	Physical modeling
13	PSD3	2 (R1 + R2)	Position 1	Physical modeling
14	PSD3	3 (R1 + R2 + R3)	Position 1	Physical modeling
15	PSD4	1 (R1)	Position 1	Physical modeling
16	PSD4	2 (R1 + R2)	Position 1	Physical modeling
17	PSD4	3 (R1 + R2 + R3)	Position 1	Physical modeling
18	PSD4	1 (R1)	Position 1	Numerical simulation
19	PSD4	2 (R1 + R2)	Position 1	Numerical simulation
20	PSD4	3 (R1 + R2 + R3)	Position 1	Numerical simulation
21	PSD4	1 (R1)	Position 2	Numerical simulation
22	PSD4	2 (R1 + R2)	Position 2	Numerical simulation
23	PSD4	3 (R1 + R2 + R3)	Position 2	Numerical simulation

equivalent shear modulus, equivalent radius, and equivalent mass, respectively; S_n and S_t are calculated by Eqs. (3) and (4); δ_n , δ_t , v_n^{rel} , and v_t^{rel} are the overlaps and relative velocities in the normal and tangential directions, respectively; μ is the coefficient of static friction; γ is calculated as follows:

$$S_n = 2 \cdot E^* \sqrt{R^* \delta_n} \tag{3}$$

$$S_t = 8 \cdot G^* \sqrt{R^* \delta_n} \tag{4}$$

$$\gamma = \frac{-\ln e}{\sqrt{\ln^2 e + \pi^2}} \tag{5}$$

where e is the restitution coefficient.

The input parameters for Eqs. (1)–(5) are listed in Table 3 and were obtained using experimental measurement and the numerical calibration process suggested by Coetzee [11]. For detailed calibration process, please refer to “Appendix A.” DEM modelling is conducted to help interpret the micro-mechanism of debris-baffle interaction, while considering the computational efficiency,

Table 3 DEM input parameters

Material parameters	Value	Contact parameters	Value
Particle diameter d_s (mm)	2–4	Coefficient of restitution e_c	0.5
Particle density ρ_s (kg/m ³)	2500	Particle friction coefficient μ_s	0.784
Young’s modulus of particle E_s (MPa)	100	Particle rolling friction coefficient μ_{rs}	0.3
Particle Poisson’s ratio ν_s	0.25	Flume friction coefficient μ_{0f}	0.457
Barrier/flume density ρ_0 (kg/m ³)	900	Barrier friction coefficient μ_{0b}	0.457
Young’s modulus of barrier/flume E_0 (GPa)	1	Flume/barrier rolling friction coefficient μ_{r0}	0.2
Poisson’s ratio of barrier/flume ν_0	0.4	Gravity g (m/s ²)	9.81

particularly for smaller particles, only the physical experiments with 2–4 mm particles are back-analyzed in the numerical tests. In total, seven simulations were conducted as presented in Table 2.

3 Numerical simulation results and interpretation

3.1 Debris-baffle interaction mechanism

With a thorough understanding of the debris-baffle interaction mechanism, particularly regarding the differences between baffle structures and check dams or flexible barriers, engineers can make better use of baffles to optimize the disaster mitigation effect. This section presents various typical experimental results of the flow regime generated by granular material with a particle size of 2–4 mm while passing through the baffle structure. The debris-baffle interaction process observed in the physical test was reconstructed using 3D DEM modeling. Additionally, the force network in the granular flow was included. The results are presented in Fig. 2. To highlight the debris-baffle interaction process, the initial time ($t = 0$ s) was adjusted to the moment when the flow front reaches the baffle. This adjustment only pertains to Fig. 2, where it can be seen that before impacting the baffle, the granular flow velocity reached 1.4 m/s ($t = 0$ s) estimated based on PIV analysis, which was reasonably captured by the DEM simulation. Moreover, it can be seen that the force chain in the flow front was sparse. At $t = 0.05$ s, some particles passed through the baffle slits and formed several separated distributaries, while the granular flow behind the baffle started to decelerate and accumulate. The force chain distribution in the material behind the baffle became denser, while that in the material passing through the baffle was much sparser. An arch structure began to emerge and became more obvious and stable at $t = 0.09$ s and $t = 0.23$ s. Simultaneously, an increasing amount of material was deposited behind the baffle owing to the loss of kinetic energy. At $t = 0.97$ s, the main body of the granular flow lost its mobility and only some discrete particles at surface kept moving. The arch structure was stable and supported the deposited material behind the baffle.

Figure 3 shows a comparison between three granular flow disaster mitigation structures. Rigid barriers (check dams) are often constructed using concrete and are well known for their enormous stiffness. These closed barrier with enormous stiffness aim at a full retention of the debris material, or at least reduce the flow volume and velocity of the overflowed material. The main mechanism of rigid barriers relies on the formation of a dead zone behind the

barrier. After the granular flow impacting on rigid barrier, the flow velocity is dramatically reduced and material is immediately deposited behind the barrier to form the dead zone. The subsequent flow first interacts with the dead zone and loses a portion of its kinetic energy through particle collision and friction, while another portion of the kinetic energy is converted into potential energy during the flow-dead zone interaction because the flow climbs up along the ramp of the dead zone. The remaining flow energy is converted into an impact force on the barrier until all material is trapped or overflow occurs. During the debris-rigid barrier interaction process, the largest portion of the granular energy is dissipated by the enhanced inter-particle interaction caused by the dead zone formation [32, 34]. The deformation of the rigid barrier only accounts for a very small part of the total energy loss of the granular flow ($< 0.0001\%$) [34]. Flexible barriers prevent granular flow disasters in a similar manner as rigid barriers. A notable difference between these two barrier types is the considerable deformation ability of the flexible barrier, and thus this barrier can absorb a portion of the granular flow energy ($< 10\%$) [34] and assist in reducing the impact load on the barrier [26]. During the debris-baffle interaction process, the arch structure, which is a typical structure in granular material [5] especially when passing a narrow space [41], plays a crucial role in the deceleration of the granular flow (Fig. 2). This is a unique flow-structure interaction mechanism and is different to that of the rigid barrier and flexible barrier. The baffle structure promotes the formation of the force arch by simultaneously changing the contact behavior of the particles in the granular flow and also provides support for the stability of the arch structure. With the break and reconstitution of the force arch, the inter-particle interaction is enhanced and thus the kinetic energy of the granular flow is reduced.

To quantitatively describe the process of granular flow deceleration caused by the baffle, we calculated the clogging time of baffle, which is defined as the time interval between the moment when the debris reaches the baffle and the moment when the particles stop moving [24]. To this end, the control volume was defined as shown in Fig. 4a. The width of the control volume was equal to the baffle spacing, the height was sufficiently large to accommodate all the passing particles, and the length was $4d_s$, determined by the radius of curvature of granular arches formed during debris-baffle interaction, where d_s is the maximum particle size used in the DEM simulation. To demonstrate the clogging capacity of different baffle arrays, a control volume was set for every single array and is denoted as C1, C2, and C3, respectively. The clogging was assessed as the existence of particles in the control volume, and the particle kinetic energy was negligible, according to the

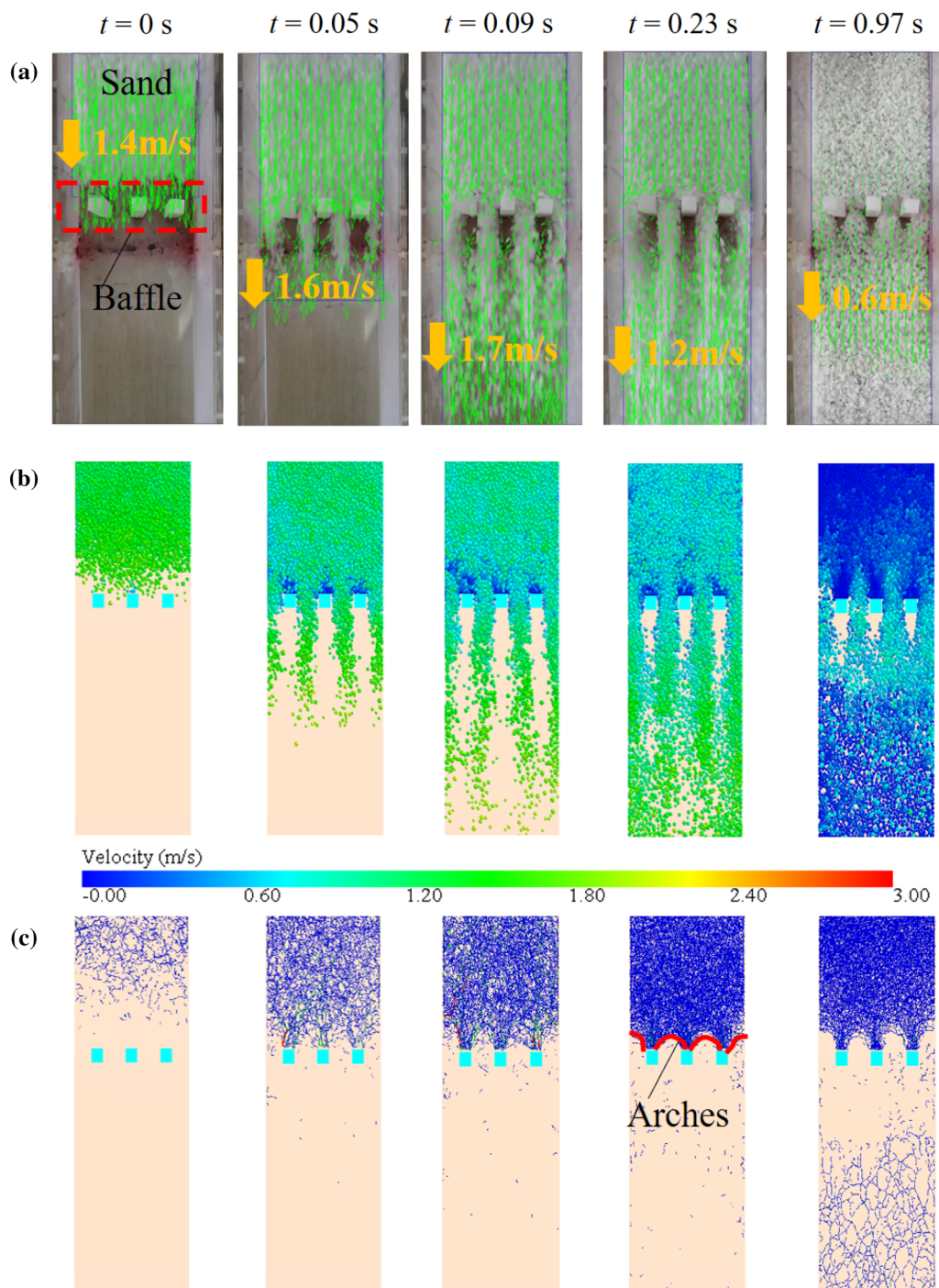


Fig. 2 Comparison of flow regime observed in **a** physical experiments and **b** numerical simulations; **c** force network distribution observed during flow-baffle interaction; the initial time was set to the time when the flowing material reached the baffle

threshold $E_{Kc} < 10^{-5}$ J used by Marchelli et al. [24]. The E_{Kc} value was calculated as follows:

$$E_{Kc} = \sum_{i=1}^k \left(\frac{1}{2} m_i v_i^2 + \frac{1}{2} I_i \omega_i^2 \right) \tag{6}$$

where k is the total particle number included in the control volume; m_i is particle mass; v_i and ω_i are, respectively, particle translational and angular velocity.

The results for the cases with three baffle arrays are presented in Figs. 4b, c and 5. Here, the initial time was set as the time when the material was released. When particles entered the control volume, the monitored particle number

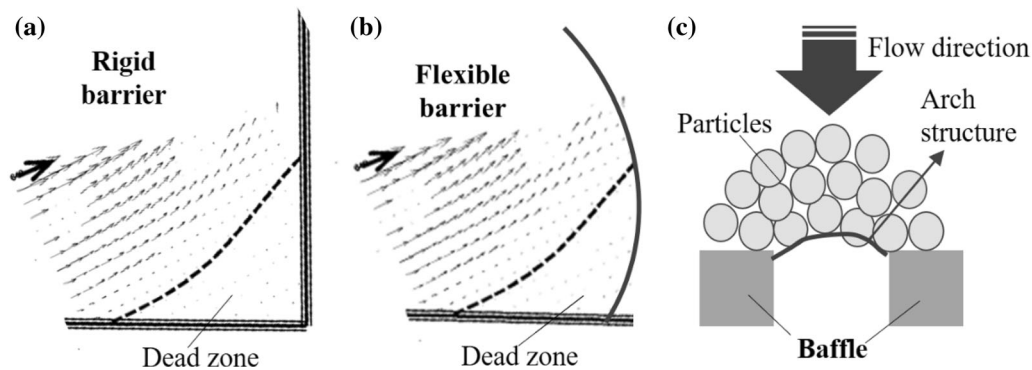


Fig. 3 Comparison of interaction mechanism between granular flow and (a) rigid barrier, b flexible barrier, and c baffle structure; the explanation of rigid barrier and flexible barrier is based on the work of Song et al. [34]

and kinetic energy dramatically increased. When the baffle was installed at the slope (position 1), the energy evolution of $C1_P1$ was much fiercer than that of $C2_P1$ and $C3_P1$. A progressive clogging phenomenon was observed throughout. When the baffle was constructed at the deposition area (position 2), only baffle $R1$ and $R2$ effectively decelerated the granular flow, and thus the result for $C3_P2$ is not shown. As shown in Fig. 5, the monitored kinetic energy and particle number of $C1_P2$ are approximately 6.99 times equal to those of $C2_P2$. This discrepancy is much more significant compared with that between $C1_P1$, $C2_P1$, and $C3_P1$.

According to the clogging time definition, we can directly detect the value from Figs. 4b, c and 5. The calculated clogging time was normalized by $\sqrt{h/g}$, where h and g are the baffle height and gravity, respectively. The normalized results are summarized in Table 4. At micro-scale, the clogging time defined here could provide some information regarding which baffle array ($R1$, $R2$, or $R3$) makes a more significant contribution during the granular flow deceleration process. With a larger clogging time, the contribution may also be larger. As presented in Table 4, the normalized clogging time for $C1_P1$, $C2_P1$, and $C3_P1$ is 17.23, 15.03, and 9.08, respectively, which indicates that $R1$ has the highest contribution to disaster reduction. The normalized clogging time for $C1_P2$ and $C2_P2$ is 19.42 and 9.71, respectively.

We defined another indicator, namely, the contribution ratio, which is calculated as the ratio of the clogging time between baffle $R1$ and the other baffle arrays (t_{c_Ri}/t_{c_Rj} , where t_c denotes clogging time and the subscript “ Ri ” and “ Rj ” represent different baffle array). As the contribution ratio became larger, the contribution of baffle $R1$ increased. The contribution ratio is important because it can be used to design a reasonable baffle configuration, wherein the contribution of each baffle array is optimal. Thus, unnecessary construction costs can be avoided. In the field, the shape and stiffness of every single baffle are the same

[6, 27, 39]. Hence, better baffle configurations have a contribution ratio close to 1, because the maximum capacity of each baffle has been utilized. For the baffles at position 1, the contribution ratio between $R1$ and $R2$ is 1.15, while that between $R1$ and $R3$ is 1.90 (Table 4). For the baffles at position 2, the contribution ratio between $R1$ and $R2$ is 2 (Table 4) with an increment of 73.91%. These results reveal that the baffle constructed at the deposition area may not be a better configuration because the contribution of baffle $R1$ is the highest and baffles $R2$ and $R3$ are not fully used.

3.2 Kinetic energy and impact force analysis

The kinetic energy of granular flow is directly related to its destructive capacity. Therefore, it is important to investigate the evolution of kinetic energy with and without a baffle structure and to determine the efficiency of the baffle. In this section, the total kinetic energy E_K , which includes the translation energy and rotation energy of the particles encompassed within the simulation domain, was calculated and is plotted in Fig. 6, which also illustrates the influence of the baffle array number and construction site. Additionally, the kinetic energy was normalized by the initial total energy of the granular assembly. As shown in Fig. 6a, under the free flow condition (no baffle), E_K increased to 25% of the initial total energy, whereas when a baffle existed, the maximum kinetic energy during the evolution process was only 6.5% of the initial total energy. The influence of the baffle array number is not very important in our case because the reduction of the maximum kinetic energy was approximately identical (20%). The reason for this is that the contribution of baffle $R1$ was always higher in the granular flow deceleration process. However, with one baffle array ($R1$) and two baffle arrays ($R1 + R2$), after the granular flow passed through the baffle, the kinetic energy of the granular flow slightly increased (1–2%) until the flow condition became gentle.

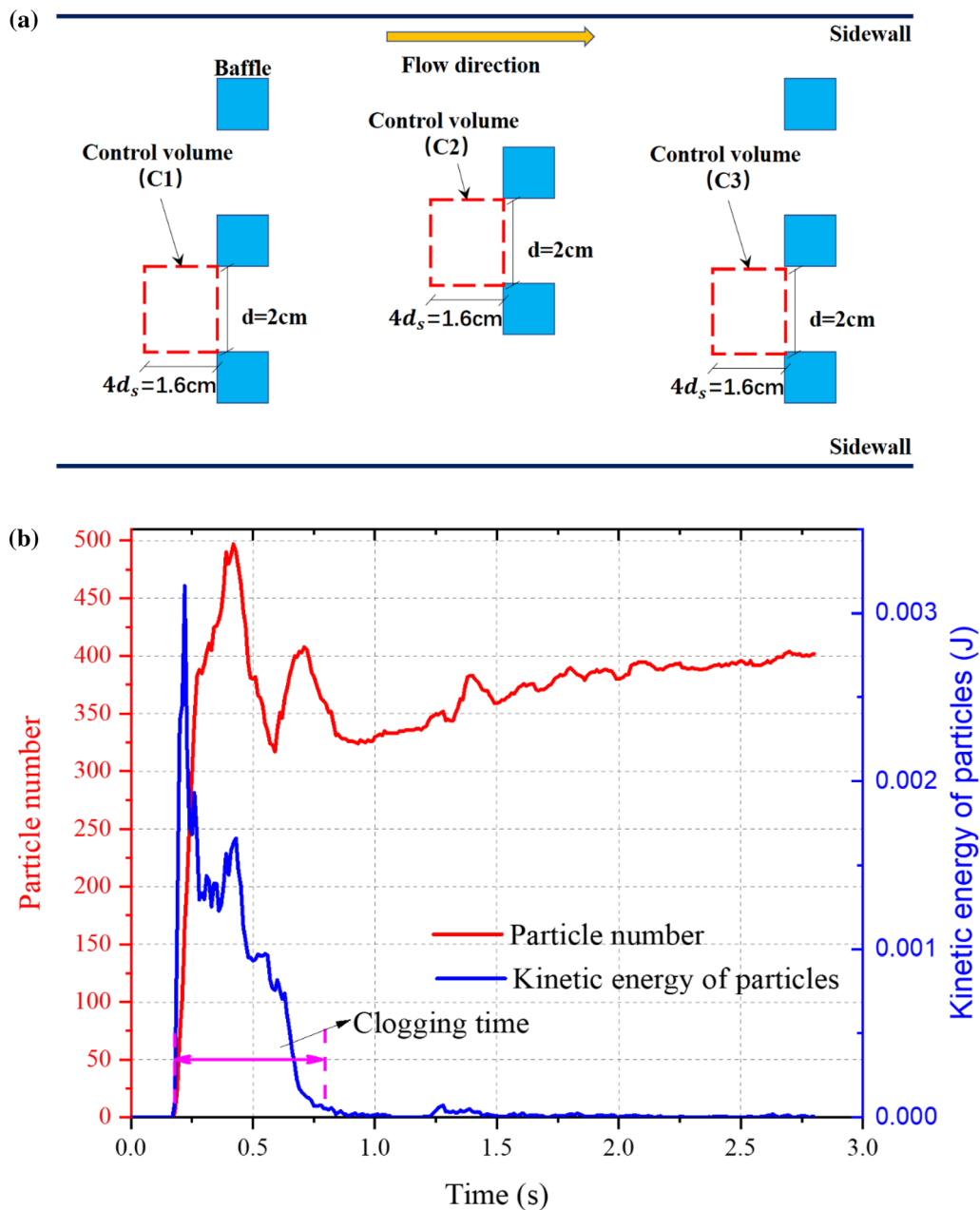


Fig. 4 Jamming characteristics of granular flow passing the baffle structure ($R1 + R2 + R3$) installed at position 1: **a** definition of control volume (C1–C3); the monitored particle number and kinetic energy within **b** C1_P1, **c** C2_P1, and **d** C3_P1 are presented; the initial time was set to the time when material was released

In field design, it is important to restrict the flow kinetic energy recovery, which reduces the baffle efficiency. Apparently, increasing the baffle array number and reasonably designing the baffle array distance can result in the gradual deceleration of the granular flow (Fig. 6a). When the baffle was constructed at the deposition area (position 2), the kinetic energy of the granular flow exhibited a different evolution pattern, as shown in Fig. 6b. The baffle exerted a slight influence on the flow's kinetic energy

evolution, and by increasing the baffle number, the time-dependent evolution trend remained approximately the same. After the peak, the kinetic energy gradually decreased by following a path like that in the free flow case, which suggests that the efficiency of the baffle structure is not obvious.

To perform a quantitative assessment, we considered the energy-breaking efficiency (E_η), which has been defined by Marchelli et al. [24] as follows:

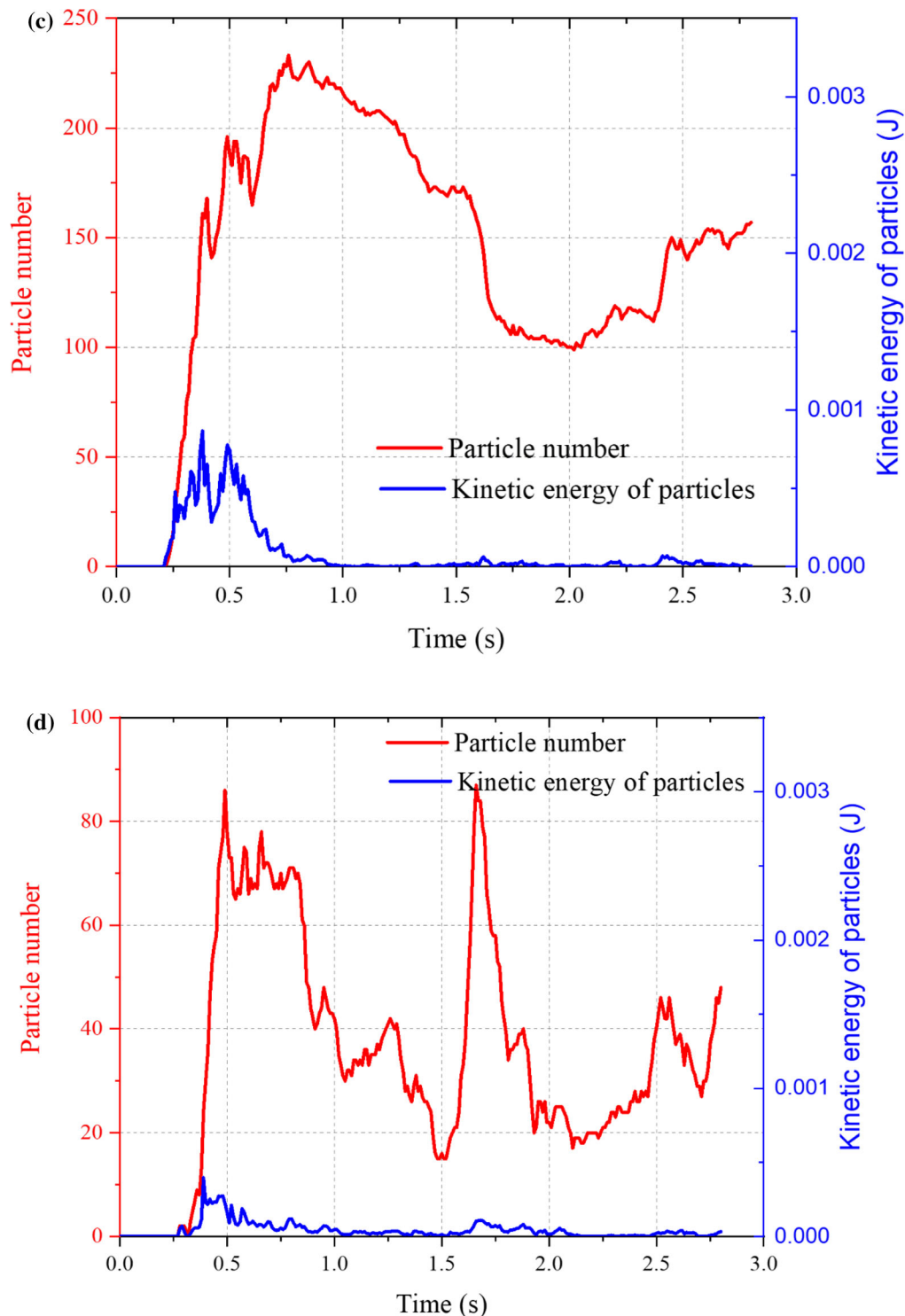


Fig. 4 continued

$$E_{\eta} = \frac{\int_{t_0}^t (E_{K_{\text{free}}} - E_{K_{\text{baffle}}}) dt}{\int_{t_0}^t E_{K_{\text{free}}} dt} \quad (7)$$

where $E_{K_{\text{free}}}$ and $E_{K_{\text{baffle}}}$ are the kinetic energy of the granular flow without and with the baffle structure,

respectively; t_0 and t are the initial time of the flow formation and the flow end time, respectively. The results are summarized in Table 5. One baffle array constructed on the slope (position 1) could reach an energy-breaking efficiency of 70.41%. Increasing the baffle array number to

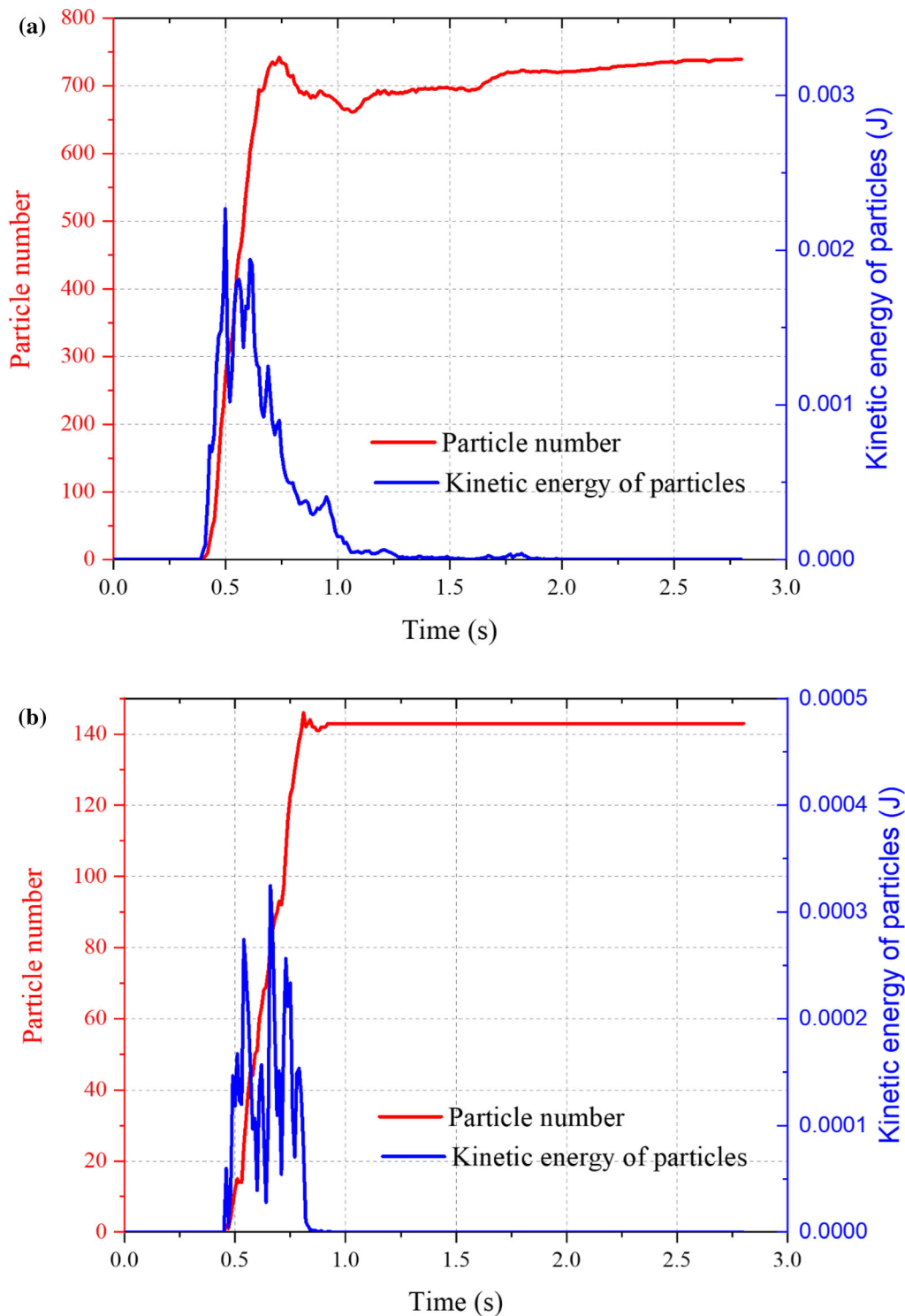


Fig. 5 Jamming characteristics of granular flow passing the baffle structure ($R1 + R2 + R3$) installed at position 2; the monitored particle number and kinetic energy within **a** C1_P2 and **b** C2_P2 are presented; the initial time was set to the time when material was released

two and three only made E_{η} increased by 3.96% and 8.41%, respectively. However, the baffles in the deposition area only generated an E_{η} of 17.66%, which is lower by 52.75% than that generated by the baffles on the slope. By

increasing the baffle array to three, the discrepancy also increases to 60.97%.

The mechanism revealed by Fig. 6b we think it is not dominated by flume length, although insufficient

Table 4 Normalized clogging time illustrating deceleration function of baffle structure. And the value in bracket gives the contribution ratio of baffle array

Baffle row	Position 1	Position 2
R1	17.23	19.42
R2	15.03 (1.15)	9.71 (2.00)
R3	9.08 (1.90)	–

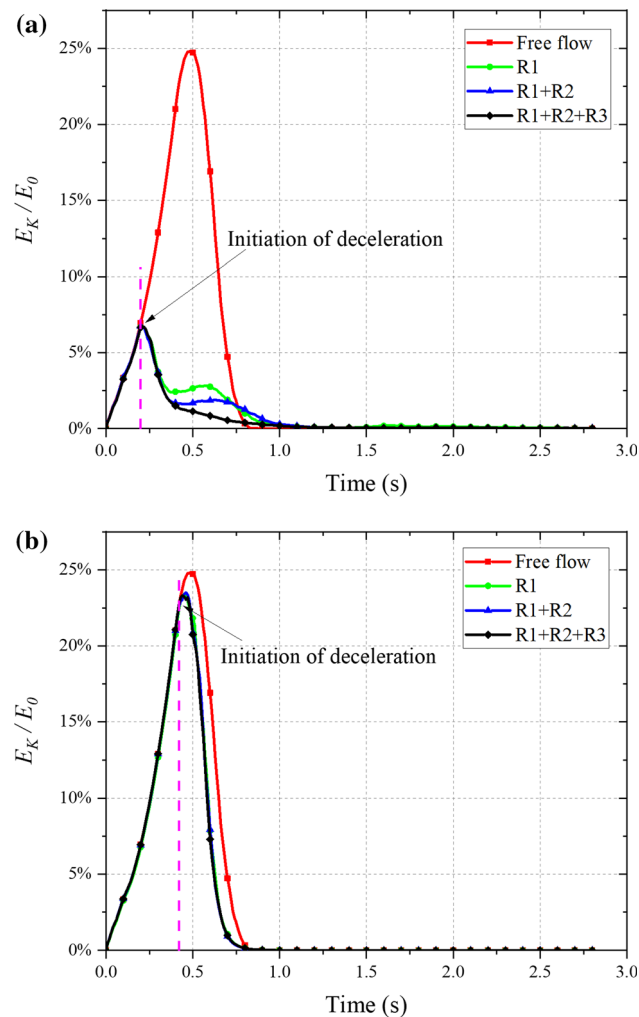


Fig. 6 Evolution of kinetic energy of granular flow: **a** the baffle is constructed at position 1 (acceleration stage) and **b** position 2 (deceleration stage). E_K -kinetic energy of granular flow; E_0 -total energy of granular assembly at initial time

interaction between granular flows and baffles at position 2 may mainly due to the short length of flume resulting in materials without sufficient acceleration to further downstream. To obtain detailed explanation, we should keep in mind that the debris-baffle interaction lies in the evolution process of the granular arches formed when granular flow passing baffle slits (Fig. 2). The stability of granular arches

Table 5 Quantification of energy-breaking efficiency (E_η) of baffle structure

Baffle row number	Position 1 (%)	Position 2 (%)
1 (R1)	70.41	17.66
2 (R1 + R2)	74.37	17.73
3 (R1 + R2 + R3)	78.82	17.85

is determined by the ratio of particles size to baffle spacing [14] in addition to the granular flow velocity [9]. With larger flow velocity, the granular arches are easy to be broken resulting lower energy-breaking efficiency of baffles. And besides, when granular flow surging downslope, the kinetic energy is monotone increasing before reaching deposition area. As a result, the baffles placed close to deposition area may start to play a role in deceleration when flow energy approaching its peak value, and because the granular flow has already been decelerated when entering deposition area, the energy loss calculated by Eq. (7) is much lower (Table 5). The above two mechanisms are the main cause of the results presented in Fig. 6. In field design, the installation of a baffle at the stage when the granular flow mobility approaches the peak should be avoided because optimal baffle performance cannot be achieved.

The baffle stability is an important consideration in engineering design. In this study, the total impact force on the baffle was calculated as follows:

$$F_{R_i} = \frac{\sum_{p=0}^q F_p}{N_i}, \quad i = 1, 2, 3 \quad (8)$$

where F_p denotes the contact force between particle p and the baffle; q is the total number of particles contacting the baffle array at a given time; N_i is the number of baffles in an array (R1, R2, or R3). Equation (8) gives the average value of the total impact force on a single baffle in an array. The results are presented in Fig. 7. The impact force on baffle R1 exhibits an obvious peak and residual characteristics, while the force impulse on baffles R2 and R3 gradually disappears. Baffle R1 is always subjected to the largest impact force, and because baffle R1 has already reduced the flow velocity, the force on baffle R2 is much lower compared with that on baffle R1 (approximately 70% for R2 at position 1, and approximately 98% for R2 at position 2). This non-uniform impact force distribution is one of the main disadvantages of the baffle structure because in current engineering practice this structure is designed with same strength regardless of whether the baffle is installed in a which array [6, 27, 39], which results in unnecessary construction costs. This problem should be highlighted in future studies and will be discussed in more

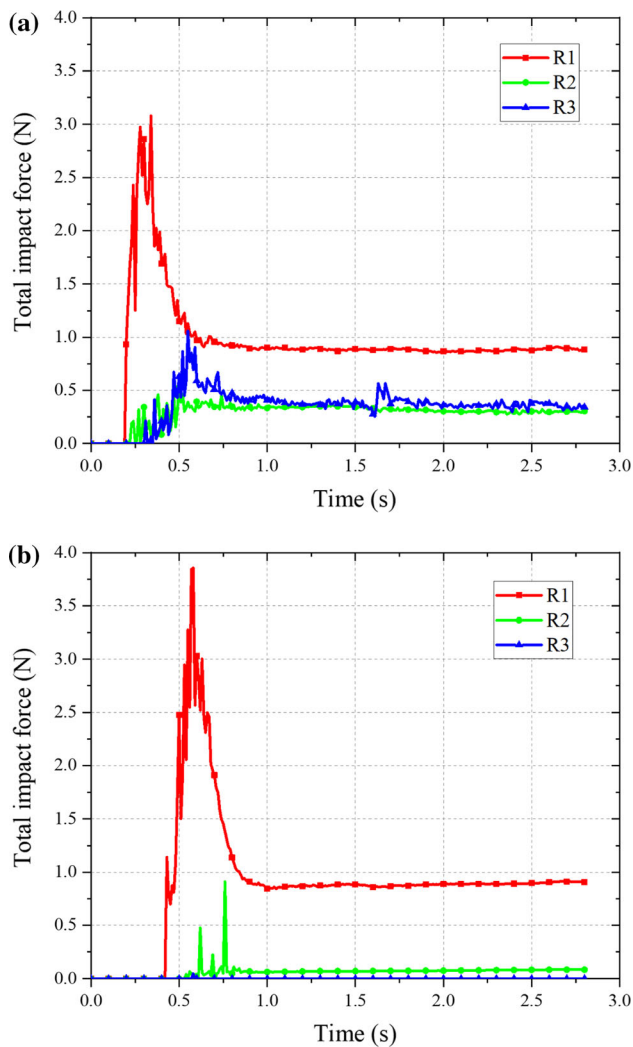


Fig. 7 Average impact force on baffle row in simulation with the baffle row number of 3. The results were obtained for the case when the baffle was installed at **a** position 1 and **b** position 2

detail below. Additionally, baffle *R1* at position 2 was subjected to a larger (e.g., the peak value is larger by approximately 30%) impact force compared with that at position 1, which again demonstrates the importance of selecting an appropriate baffle construction site.

3.3 Run-out and deposition analysis

This section provides a full analysis with regard to the run-out and deposition characteristics of granular flow, which are simultaneously affected by the baffle array number, particle size effect and construction site effect.

Every flow case was recorded using the same camera fixed immediately above the deposition area. To better interpret the experimental results, we adopted a transparent plate to serve as the deposition area, and another thin plate plotted with a reference grid (5×5 cm) was placed under

the deposition area. Hence, the location of the debris material could be easily tracked. The final deposition shapes of the different flow cases were directly compared using the captured images. The comparison is presented in Fig. 8, and the outlines of the deposited material are indicated by the colored dash lines. The spreading morphology of the debris deposited on the slope under different experimental conditions was compared in the same manner, as shown in Fig. 9. Two indices are used to describe the granular flow deposition characteristics, namely, the run-out distance (L_d) on the deposition area defined as the central distance from the slope toe to the front of the deposition, and the spreading distance (L_s) on the slope defined as the central distance from the slope toe to the tail of the deposition. With a lower run-out distance and larger spreading distance, the efficiency of the deceleration effect exerted by the baffle structure is better. The reduction of the run-out distance and spreading distance caused by the baffles was calculated in a normalized format as follows. The results are presented in Tables 6 and 7.

$$L_{d\eta} = \frac{L_{d\text{free}} - L_{d\text{baffle}}}{L_{d\text{free}}} \quad (9)$$

$$L_{s\eta} = \frac{L_s}{L_{s\text{slop}}} \quad (10)$$

where the subscripts “ η ,” “free,” and “baffle” denote the normalized value, the results without the baffle structure, and the results with the baffle structure, respectively; $L_{s\text{slop}}$ is the slope length (80 cm).

In Fig. 8, an overall fan-shaped deposition can be observed. After the granular flow reaching the deposition area, because the lateral confinement immediately vanished, the flow moved forward and spreaded laterally, which generated a fan-shaped deposition. At the end of the flow, the lateral extension became much more obvious at the end of deposition owing to the combined effect of the lower flow velocity and dead debris generated by the previous flow. While when the particle size is increased from 0.1–0.5 mm to 2–4 mm, the enhanced lateral extension at the end of the deposition gradually disappeared. The particle size appeared to influence the flow mobility. As shown in Figs. 8 and 9, the run-out distance (L_d) of the 2–4 mm particles was larger than that of the 0.1–0.5 mm particles by approximately 17%, while the spreading distance (L_s) was lower by approximately 10%.

The baffles installed on the slope (position 1) exerted considerable influence on the granular flow deposition characteristics. After passing through the baffle structure, the granular flow exhibited similar deposition manner but with a largely reduced axial run-out distance and lateral extension (Fig. 8). As presented in Table 6, baffle *R1* reduced the L_d of PSD1 by 38% compared with the free

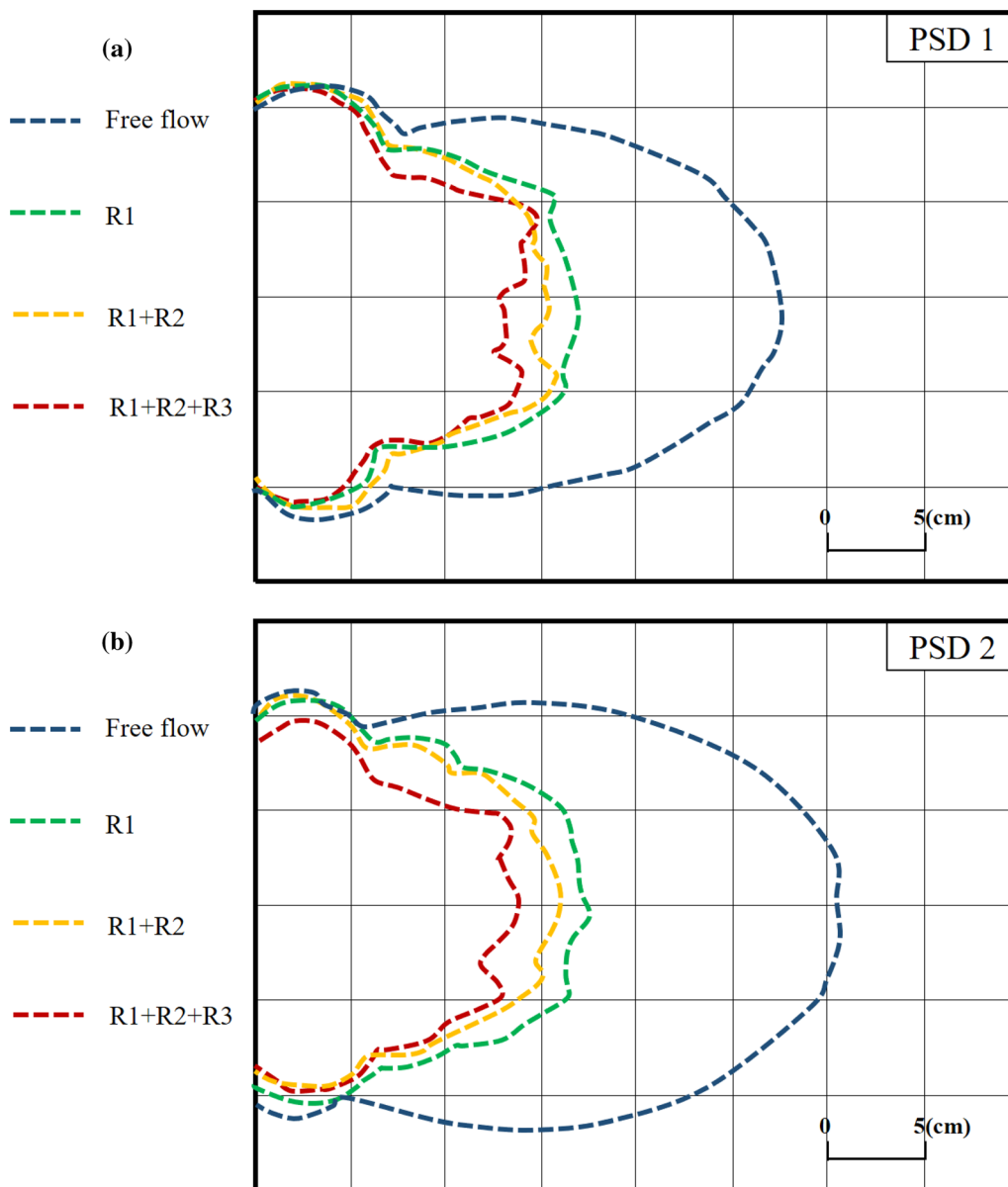


Fig. 8 Morphology of granular material deposition after passing baffle structure installed at position 1; the effect of the baffle row number and particle size are included: **a** PSD1, **b** PSD2, **c** PSD3, and **d** PSD4

Table 6 Reduction of run-out distance of granular flow by baffle structure

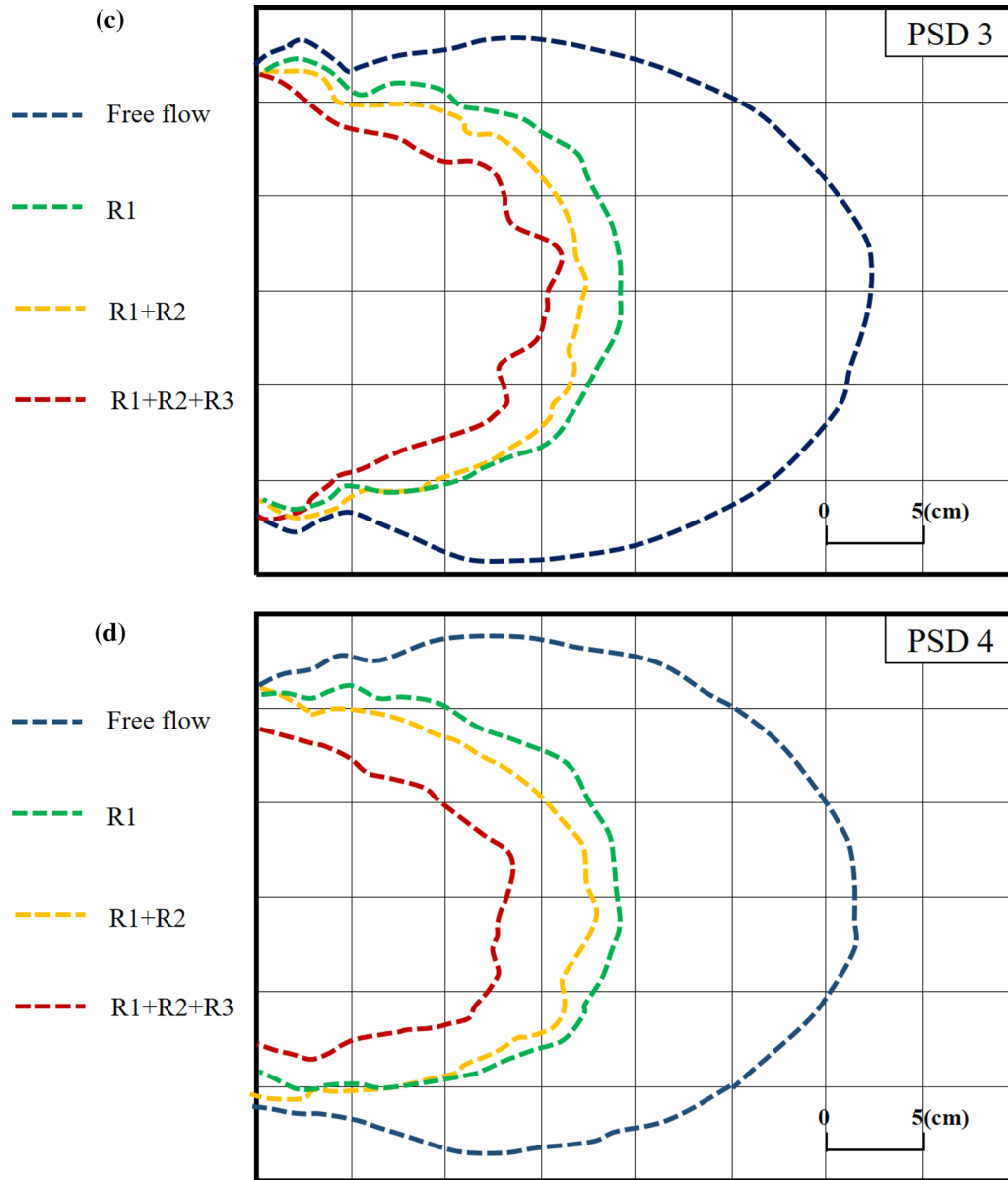
Material	R1 (%)	R1 + R2 (%)	R1 + R2 + R3 (%)
PSD1	38	43	46
PSD2	42	48	54
PSD3	40	45	50
PSD4	39	43	57

flow condition. By increasing the baffle array number from 1 to 3, the reduction of L_d increased up to 46% with an

increment of approximately 8%. However, when larger particles are considered (PSD4), baffle R1 generated an $L_{d_{\eta 1}}$ that is comparable to that of PSD1, while three baffle arrays caused the $L_{d_{\eta 1}}$ to increase by 18%, which is larger than the 8% increase of PSD1. The results of $L_{s_{\eta 1}}$ exhibit a similar trend. Owing to the presence of the baffle structure, the spreading distance of the debris deposition of PSD1 on the slope increased by 30%, 37.5%, and 46.25% with one, two, and three baffle arrays, respectively. For PSD4, these increments were 52.50%, 58.75%, and 67.5%. The definition of L_s does not illustrate the flow mobility in the same way as L_d . With a larger L_s , more materials are deposited on the slope, which is dangerous in the field and requires

Table 7 Normalized spreading distance of granular material on slope

Material	Free flow (%)	R1 (%)	R1 + R2 (%)	R1 + R2 + R3 (%)
PSD1	21.25	51.25	58.75	67.50
PSD2	17.50	61.75	67.50	78.75
PSD3	17.50	63.43	68.75	82.50
PSD4	11.25	63.75	70.00	78.75

**Fig. 8** continued

caution because these loose materials can easily transform into debris flow when rainstorms occur and can even cause severe disasters.

The results presented in Tables 6 and 7 demonstrate that the particle size and baffle array number are both crucial considerations in baffle design. The influence of the baffle array number is directly related to the energy-breaking

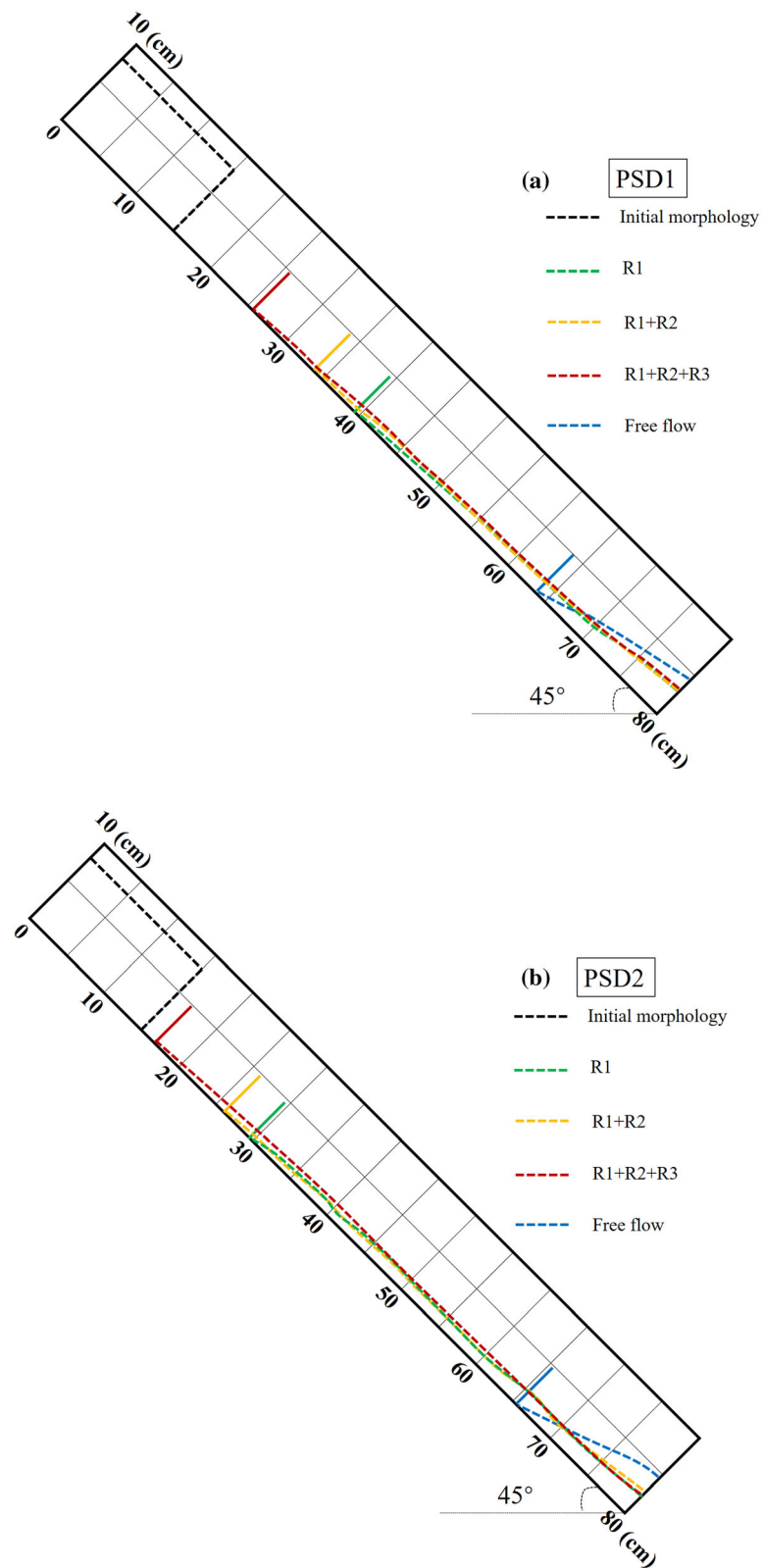


Fig. 9 Spreading morphology on slope of granular material after passing the baffle structure installed at position 1; the effect of the baffle row number and particle size are included: **a** PSD1, **b** PSD2, **c** PSD3, and **d** PSD4. Note: the solid lines in figure mark the deposition tail

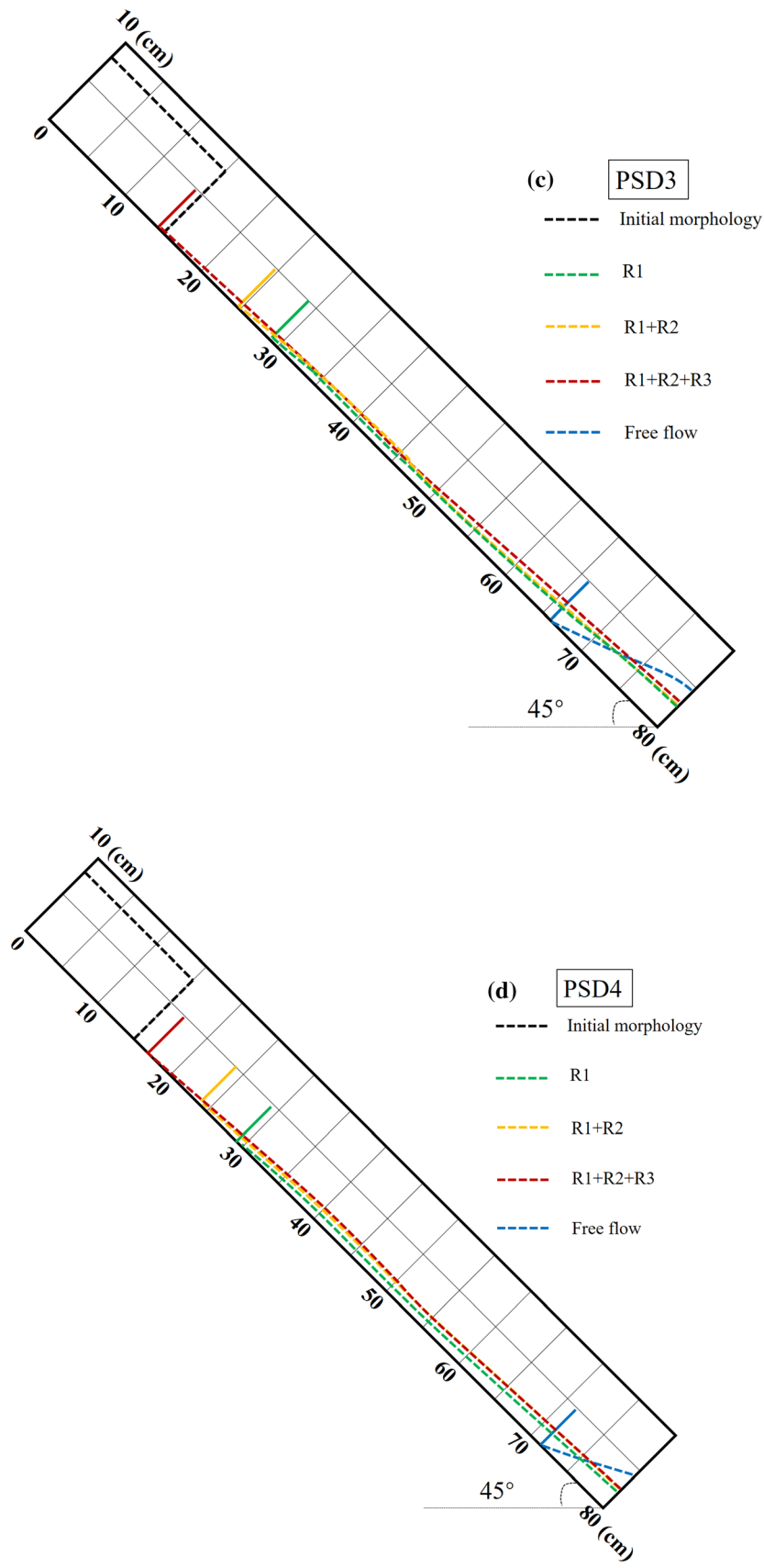


Fig. 9 continued

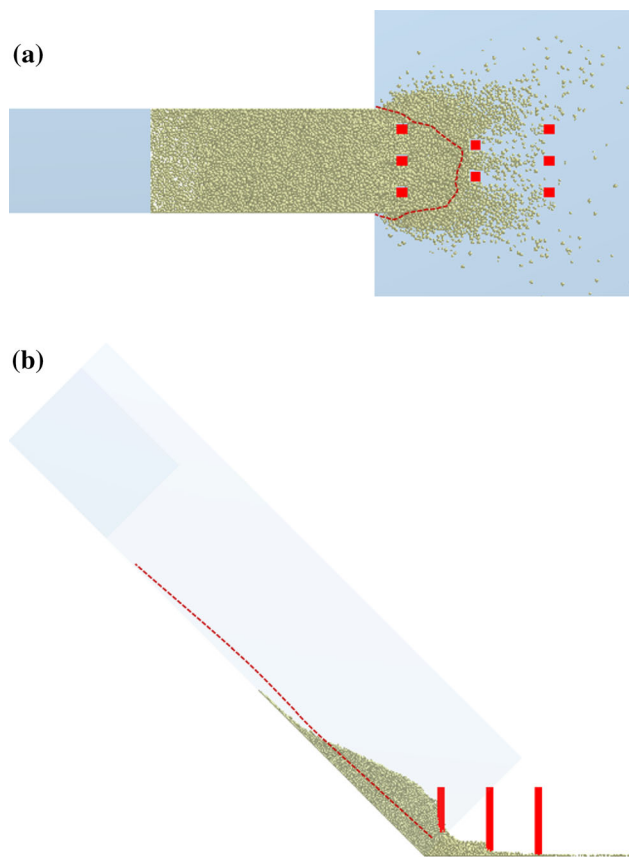


Fig. 10 **a** Final deposition of granular material after passing three rows of baffles installed at position 2; **b** spreading morphology on slope of granular material after passing three rows of baffles installed at position 2; the red dash line represents the result obtained from physical experimental tests for the case of three rows of baffles installed at position 1

efficiency of the baffles, as has already been discussed. The particle size effect is controlled by the jamming behavior. When a granular flow passes through a narrow spacing, the particle contact behavior may change, and with the support from the baffle, force arches are formed (Fig. 2) and interact with the subsequent flows, which results in the dissipation of kinetic energy. Larger particles can facilitate

the rapid formation of a stable force arch with larger energy-breaking efficiency, and thus larger L_{d_n} . The jamming characteristics explain the results presented in Table 6, while the comparable L_{d_n} , when one and two baffle arrays are considered, is attributed to the recovery of the kinetic energy after the granular flow passing the baffle, as mentioned above. The reason for this is that larger particles always had larger mobility in this study. Additionally, it was observed that the particle size (PSD1 is 0.1–0.5 mm, PSD2 is 0.5–1 mm, PSD3 is 1–2 mm, and PSD4 is 2–4 mm) of the granular material used in the experimental tests monotonically increased, but L_{d_n} did not exhibit a monotonically increasing trend. This phenomenon highlights the complexity of the debris-baffle interaction. Although a detailed explanation of the debris-baffle interaction mechanism has been provided, the particle size effect is still difficult to describe in quantitative terms. Nevertheless, some qualitative knowledge can still be obtained. Specifically, there may be a critical particle size below which the particle size does not significantly affect the baffle efficiency, but the determination of this critical value relies on which aspect of the baffle performance is considered (energy-break efficiency or deposition regulation).

To illustrate the influence of the baffle construction site on the deposition behavior of granular flow, the experimental results and numerical results for a flow with a particle size of 2–4 mm (PSD4) are presented in Fig. 10. Obviously, the energy-breaking efficiency of baffles at position 2 is lower compared with that at position 1, particularly about the run-out distance (L_{d_n} is larger by approximately 10%) and spreading distance on the slope (L_{s_n} is lower by approximately 40%). The reason for this may be that the baffles at position 2 were not fully used because baffle R3 was useless in our simulation. Figure 11 shows the influence of the baffle array number on the granular flow deposition. Most material was deposited at the slope toe and formed a bluff-shaped side view of the

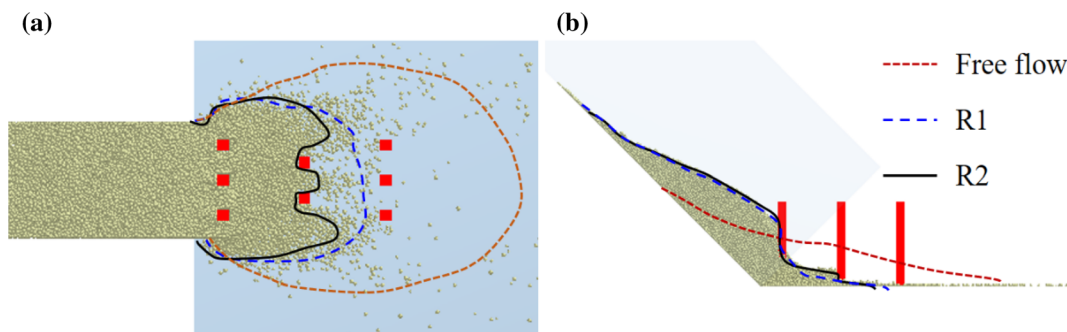


Fig. 11 Deposition morphology of PSD4 after passing baffle structure installed at position 2; the effect of the baffle row number is included: **a** plain view and **b** side view

deposition. Additionally, the baffle array number did not exert substantial influence on L_{d_n} and L_{s_n} .

4 Discussion

4.1 Model limitations

The model scale effect and interstitial fluid effect are two important limitations in our experimental and numerical tests. The scale effect is an important consideration when conducting physical modelling. And it is also a technical challenge to achieve similitude between model and prototype flows. Though scale effect cannot be avoided, small-scale flume tests still play an important role in investigation of flow-structure interaction-related problem because of economic efficiency and excellent controllability in testing conditions [20, 25, 26, 39]. In our tests, dry granular flows are considered. And according to the widely accepted agreement reported in the literature, Froude number ($F_r = v/\sqrt{gh}$, where v is the flow front velocity, g is the gravity, and h is the flow depth) could be used to guarantee dynamic similarity of granular flows [9, 14, 20, 26, 32, 41]. In our physical modelling, the generated F_r is approximately 3.1 for the baffles at position 1, and 4 for the baffles at position 2. Therefore, the proposed model is suitable to dry granular flows with similar F_r . However, according to the results presented in submitted manuscript, the stability of granular arches formed during debris-baffle interaction is also sensitive to flow velocity. And thus, our results should be further verified when superspeed granular flow is considered. For such a purpose, centrifuge modelling considering the high-speed nature of granular flows [34] and numerical simulations taking topography into consideration [8] should be encouraged while beyond the scopes of this paper. Additionally, the inter-particle interaction and debris-barrier interaction are largely affected by the interstitial fluid, which weakens the frictional behavior of granular matter owing to the lubrication effect. Thus, the force network changes and the debris-baffle interaction mechanism can no longer be controlled by the force arch structure. Hence, our results are more suitable to arid regions, where dry granular flow disasters are prevalent.

4.2 Future work

Baffles have been demonstrated to be an effective measure both at laboratory scale and field scale [6, 10, 21, 23, 27, 39]. However, various important issues remain unresolved. In this regard, at least two aspects should be highlighted. On one hand, almost all existing relevant studies, including this study, have considered

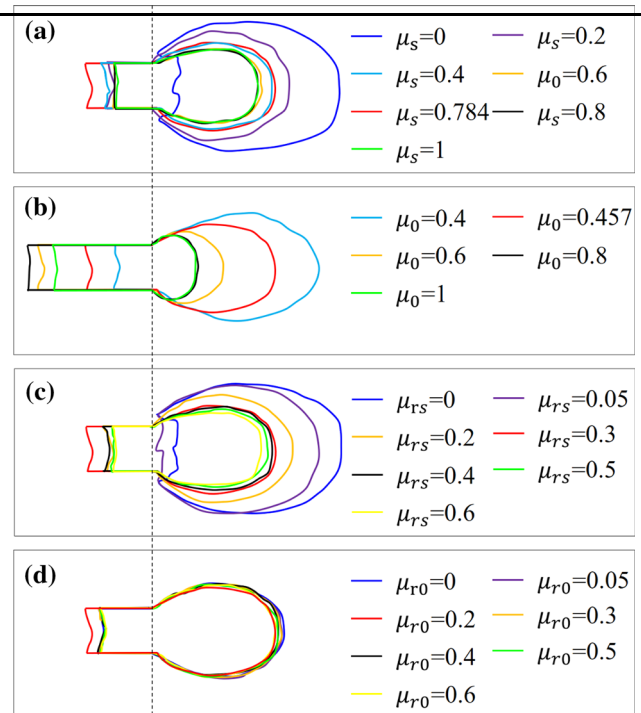


Fig. 12 Sensitivity analysis of DEM input parameters. **a** Particle friction coefficient μ_s , **b** flume/barrier friction coefficient μ_0 , **c** particle rolling friction coefficient μ_{rs} , **d** flume/barrier rolling friction coefficient μ_{r0}

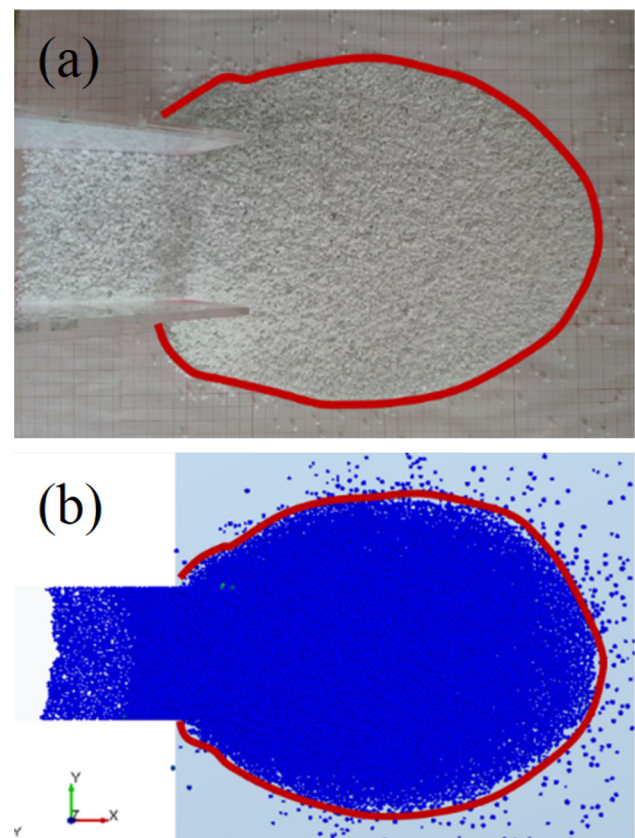


Fig. 13 Deposition morphology comparison between (a) physical modelling result and (b) numerical simulation result

baffles that cannot be destroyed. However, actual engineering structures in the field will bend and even fail. The baffle shape and dimensions do not only affect the baffle's disaster mitigation capability but also its flexural rigidity and failure potential. Hence, in future work, the baffle performance should be assessed with consideration to the destruction process. Thus, the baffle configuration (for example, the height) can be better determined. On the other hand, existing studies have tended to determine the optimal baffle configuration under specific disaster scenarios, without much consideration given to optimization design. This paper highlights the importance of adopting a baffle configuration with a better contribution ratio (approaching unity) and lower impact force discrepancy on different baffle arrays, because a single baffle is constructed with same dimensions and strength. Additionally, the optimization of the baffle spacing, array distance, and baffle dimension must consider the economic cost instead of simply attempting to maximize the disaster mitigation effect.

5 Conclusion

Baffle design in the field is important for preventing high-speed granular flow disasters but challenged. This paper focuses on the mechanism of debris-baffle interaction at grain scale and tries to reveal the effect of the unsteady nature of granular flow on debris-baffle interaction. The main conclusions drawn from this study are as follows:

- (1) With the perturbation and support of the baffle, an arch structure comprising tightly contacted particles is formed between the baffles. The interaction between the arches and subsequent flows results in the breaking and reconstitution of the force arch, which serves as the main mechanism of debris-baffle interaction. This mechanism is somewhat different from the dead zone-dominant debris-barrier interaction mechanism represented by a rigid or flexible barrier.
- (2) Baffles decelerate granular flow at different stage could exhibit distinct energy evolution pattern. The baffles on the slope decelerated the granular flow in the middle stage before the flow energy reached the peak, while the baffles on the deposition area only started to work close to the peak of kinetic energy. Hence, the former baffle configuration generated energy dissipation that was 78.82% of the free flow kinetic energy, which is 60.97% larger than the latter configuration.
- (3) Froude characteristics exert important influence on baffle performance. And because that different Froude number could be identified at different stage of granular flow when surging downslope, the energy-breaking efficiency of the baffles in the deposition area was lower compared with those on the slope, particularly with regard to the run-out distance ($L_{d_η}$ was larger by approximately 10%) and spreading distance on the slope ($L_{s_η}$ was lower by approximately 40%).
- (4) The particle size and baffle array number are both crucial considerations in baffle design for reducing the run-out distance (L_d) and spreading distance (L_s) of the granular flow. With more baffle arrays, the flow mobility recovery after the flow passes the baffle structure can be avoided. The particle size effect was controlled by the baffle jamming behavior. Larger particles facilitated the rapid formation of a stable force arch with larger energy-breaking efficiency. Notably, there may exist a critical particle size below which the particle size does not significantly affect the baffle efficiency.
- (5) Gradually jamming process of baffles in deceleration of granular flows is identified, which results in the much different contribution of baffle arrays and also a non-uniform impact force distribution on baffle arrays. The contribution of baffle *R1* was 1.9 times as large as that of baffle *R3* on the slope, and the contribution discrepancy between *R1* and *R2* of baffles on deposition area is larger by 73.91% than that on slope. In addition, the impact force on *R2* was lower by 70% compared with that on *R1* for the baffles on the slope, and lower by 98% for the baffle in the deposition area.

Appendix

Appendix A Calibration of DEM model

In this Appendix, we will show the principles for selecting DEM input parameters (Table 3), which could be divided into two groups: material parameters and contact parameters.

Material parameters including particle diameter, density, Young's modulus and Poisson's ratio. In our physical experiments, quartz sand with different diameters is used, and thus in addition to Young's modulus of particles, other mentioned material parameters presented in Table 3 are selected based on the true values. Because the DEM simulation time is significantly affected by particle's Young's modulus, a practical way to save computation time is by

reducing the particle's Young's modulus, and the effectiveness of such a strategy has been demonstrated by Shen et al. [32], Jiang et al. [19], Law et al. [21], Bi et al. [6] and Choi et al. [10].

Contact parameters are used to calculate the contact force between particles or between particle and geometry. As shown in Table 3, mainly five parameters should be carefully selected. The coefficient of restitution of quartz sand particles usually is about 0.5 [19, 21, 32, 36]. And the other four parameters are calibrated based on physical experiment results. Before physical test, the frictional parameters are measured including internal friction angle of sand particles and interface friction angle of flume or baffle. Some research works treated these two macro-parameters as the micro-friction coefficient in DEM simulation [14, 19, 32, 41], while Ceccato et al. [7] think the DEM inter-particle friction angle is not equal to the measured bulk friction angle of sand assembly, because the former is a micro-parameter, and the latter is macro-representation of inter-particle interaction at micro-scale. In DEM simulation, static friction and rolling friction are both needed, and the rolling friction is often used to compensate the friction alteration because of the simplification of particle shape in DEM [36]. According to Coetzee [11], different combination of DEM contact parameters could lead to similar bulk response of granular material, and such a strategy is practical in DEM simulation, because the micro-parameters can be determined by matching the macro-behavior of granular material. We firstly conduct sensitivity analysis of particle friction coefficient μ_s , flume/barrier friction coefficient μ_0 , particle rolling friction coefficient μ_{rs} and flume/barrier rolling friction coefficient μ_{r0} . The results are shown in Fig. 12, and we can observe that μ_0 exerts the most significant influence on deposition of granular flow and the influence of μ_{r0} is smaller. Through comparison of the deposition shape between physical experimental result and DEM simulation result (Fig. 13), a proper combination of DEM contact parameters is determined (Table 3) and further used to investigate the debris-baffle interaction behavior.

Acknowledgements This study was supported by the National Natural Science Foundation of China (Grant No. 41831291).

References

- Ahmadipur A, Qiu T (2018) Impact force to a rigid obstruction from a granular mass sliding down a smooth incline. *Acta Geotech* 13(6):1433–1450
- Albaba A, Lambert S, Kneib F, Chareyre B, Nicot F (2017) DEM modeling of a flexible barrier impacted by a dry granular flow. *Rock Mech Rock Eng* 50(11):3029–3048
- Albaba A, Lambert S, Nicot F, Chareyre B (2015) Relation between microstructure and loading applied by a granular flow to a rigid wall using DEM modeling. *Granular Matter* 17(5):603–616
- Armanini A, Dellagiacomma F, Ferrari L (1991) From the check dam to the development of functional check dams. In: *Fluvial hydraulics of mountain regions*, pp 331–344
- Azema E, Radjai F (2012) Force chains and contact network topology in sheared packings of elongated particles. *Phys Rev E* 85(3):031303
- Bi YZ, Du YJ, He SM, Sun XP, Wang DP, Li XP, Liang H, Wu Y (2018) Numerical analysis of effect of baffle configuration on impact force exerted from rock avalanches. *Landslides* 15(5):1029–1043
- Ceccato F, Redaelli I, di Prisco C, Simonini P (2018) Impact forces of granular flows on rigid structures: comparison between discontinuous (DEM) and continuous (MPM) numerical approaches. *Comput Geotech* 103:201–217
- Chen HX, Li J, Feng SJ, Gao HY, Zhang DM (2019) Simulation of interactions between debris flow and check dams on three-dimensional terrain. *Eng Geol* 251:48–62
- Choi CE, Goodwin GR, Ng CWW, Cheung DKH, Kwan JSH, Pun WK (2016) Coarse granular flow interaction with slit structures. *Géotech Lett* 6(4):267–274
- Choi CE, Ng CWW, Law RPH, Song D, Kwan JSH, Ho KKS (2015) Computational investigation of baffle configuration on impedance of channelized debris flow. *Can Geotech J* 52(2):182–197
- Coetzee CJ (2017) Review: calibration of the discrete element method. *Powder Technol* 310:104–142
- Cundall PA, Strack ODL (1979) Discrete numerical-model for granular assemblies. *Geotechnique* 29(1):47–65
- Dowling CA, Santi PM (2014) Debris flows and their toll on human life: a global analysis of debris-flow fatalities from 1950 to 2011. *Nat Hazards* 71(1):203–227
- Goodwin GR, Choi CE (2020) Slit structures: Fundamental mechanisms of mechanical trapping of granular flows. *Comput Geotech* 119:103376
- He S, Liu W, Li X (2016) Prediction of impact force of debris flows based on distribution and size of particles. *Environ Earth Sci* 75(4):298
- Hu KH, Cui P, Zhang JQ (2012) Characteristics of damage to buildings by debris flows on 7 August 2010 in Zhouqu, Western China. *Nat Hazard* 12(7):2209–2217
- Huang Y, Zhang B (2020) Challenges and perspectives in designing engineering structures against debris-flow disaster. *Eur J Environ Civil Eng*
- Huang Y, Zhang B, Zhu C (2021) Computational assessment of baffle performance against rapid granular flows. *Landslides* 18(1):485–501
- Jiang YJ, Fan XY, Li TH, Xiao SY (2018) Influence of particle-size segregation on the impact of dry granular flow. *Powder Technol* 340:39–51
- Jiang YJ, Towhata I (2013) Experimental study of dry granular flow and impact behavior against a rigid retaining wall. *Rock Mech Rock Eng* 46(4):713–729
- Law RPH, Choi CE, Ng CWW (2016) Discrete-element investigation of influence of granular debris flow baffles on rigid barrier impact. *Can Geotech J* 53(1):179–185
- Leonardi A, Goodwin GR, Pirulli M (2019) The force exerted by granular flows on slit dams. *Acta Geotech* 14(6):1949–1963
- Li X, Yan Q, Zhao S, Luo Y, Wu Y, Wang D (2020) Investigation of influence of baffles on landslide debris mobility by 3D material point method. *Landslides* 17:1129–1143
- Marchelli M, Leonardi A, Pirulli M, Scavia C (2020) On the efficiency of slit-check dams in retaining granular flows. *Géotechnique* 70(3):226–237

25. Moriguchi S, Borja RI, Yashima A, Sawada K (2009) Estimating the impact force generated by granular flow on a rigid obstruction. *Acta Geotech* 4(1):57–71
26. Ng CWW, Choi CE, Koo RCH, Goodwin GR, Song D, Kwan JSH (2018) Dry granular flow interaction with dual-barrier systems. *Geotechnique* 68(5):386–399
27. Ng CWW, Choi CE, Song D, Kwan JSH, Koo RCH, Shiu HYK, Ho KKS (2014) Physical modeling of baffles influence on landslide debris mobility. *Landslides* 12(1):1–18
28. Nicot F, Cambou B, Mazzoleni G (2001) From a constitutive modelling of metallic rings to the design of rockfall restraining nets. *Int J Numer Anal Meth Geomech* 25(1):49–70
29. Remaître A, van Asch TWJ, Malet JP, Maquaire O (2008) Influence of check dams on debris-flow run-out intensity. *Nat Hazards Earth Syst Sci* 8(6):1403–1416
30. Remaitre A, Malet J (2010) The effectiveness of torrent check dams to control channel instability: example of debris-flow events in clay shales. In: *Check dams, morphological adjustments and erosion control in torrential streams*. Nova Science Publishers Inc., New York, pp 211–237
31. Roessler T, Katterfeld A (2018) Scaling of the angle of repose test and its influence on the calibration of DEM parameters using upscaled particles. *Powder Technol* 330:58–66
32. Shen WG, Zhao T, Zhao JD, Dai F, Zhou GGD (2018) Quantifying the impact of dry debris flow against a rigid barrier by DEM analyses. *Eng Geol* 241:86–96
33. Song D, Choi CE, Ng CWW, Zhou GGD, Kwan JSH, Sze HY, Zheng Y (2019) Load-attenuation mechanisms of flexible barrier subjected to bouldery debris flow impact. *Landslides* 16(12):2321–2334
34. Song D, Zhou GGD, Xu M, Choi CE, Li S, Zheng Y (2019) Quantitative analysis of debris-flow flexible barrier capacity from momentum and energy perspectives. *Eng Geol* 251:81–92
35. Take WA (2015) Thirty-sixth Canadian geotechnical colloquium: advances in visualization of geotechnical processes through digital image correlation. *Can Geotech J* 52(9):1199–1220
36. Utili S, Zhao T, Houlsby GT (2015) 3D DEM investigation of granular column collapse: evaluation of debris motion and its destructive power. *Eng Geol* 186:3–16
37. Vagnon F, Segalini A (2016) Debris flow impact estimation on a rigid barrier. *Nat Hazard* 16(7):1691–1697
38. Volkwein A, Schellenberg K, Labiouse V, Agliardi F, Berger F, Bourrier F, Dorren LKA, Gerber W, Jaboyedoff M (2011) Rockfall characterisation and structural protection: a review. *Nat Hazard* 11(9):2617–2651
39. Wang DP, Li QZ, Bi YZ, He SM (2020) Effects of new baffles system under the impact of rock avalanches. *Eng Geol* 264:105261
40. Yin Y, Li B, Wang W, Zhan L, Xue Q, Gao Y, Zhang N, Chen H, Liu T, Li A (2016) Mechanism of the December 2015 catastrophic landslide at the shenzhen landfill and controlling geotechnical risks of urbanization. *Engineering* 2(2):230–249
41. Zhou GGD, Du JH, Song DR, Choi CE, Hu HS, Jiang CH (2019) Numerical study of granular debris flow run-up against slit dams by discrete element method. *Landslides* 17(3):585–595

Publisher's Note Springer Nature remains neutral with regard to jurisdictional claims in published maps and institutional affiliations.